Phenome-scale causal inference with bidirectional mediated Mendelian randomization

Brielin C. Brown [*1, 2] and David A. Knowles [†2, 3, 4]

[1]*Data Science Institute, Columbia University, New York, NY*
[2]*New York Genome Center, New York, NY*
[3]*Department of Computer Science, Columbia University, New York, NY*
[4]*Department of Systems Biology, Columbia University, New York, NY*

May 25, 2020

Abstract

1 Introduction

Recent developments in the understanding of complex-trait genetics have lead to a call for increased study of biological networks (CITE omnigenics 1-2, visscher). However, interrogating the structure of networks is notoriously difficult, owing to factors such as unmeasured confounding and reverse causation (CITE?). In spite of these challenges, modern population-scale biobanks offer unprecedented opportunity to study biological networks because they can contain simultaneous measurements of traits, molecular markers and genetic variation (CITE ukbb, bbjp).

Mendelian randomization (MR) has recently received increased attention as a class of methods that can mitigate issues in causal inference by using genetic variants (SNPs) from genome-wide association studies (GWAS) as instrumental variables to determine the effect of an exposure (A) on an outcome (B). To estimate causal effects, MR methods must make strong assumptions that limit their ability to be applied at biobank-scale. Perhaps the most controversial assumption is that the SNP only effects B through A (*i.e.* there is no horizontal pleiotropy). Recent methods such as Egger regression and the mode-based-estimator are able to relax this assumption, instead assuming there is no correlated pleiotropy or modal pleiotopy, respectively (CITE egger, mbe). Another approach, the latent causal variable (LCV) model, is able to detect genetic causality under arbitrarily-structured pleiotropy (CITE LCV). However, the quantity that LCV calculates is not interpretable as the causal effect size of A on B. Most MR studies also presuppose the direction of effect, specifying one phenotype as the outcome and the other as the exposure. This is sound when the outcome is clearly biologically downstream of the exposure, but in many cases it is better to learn the direction of the effect from the data. Some researchers have instead used bi-directional MR (gwas-pw) (CITE bimr, pickrell). However, the utility of this approach for complex traits, which might contain non-causal genetic correlation, is questionable (CITE LCV).

In mimicking a randomized controlled trial, MR estimates the total causal effect (TCE) of A on B (CITE ??). This effect may be mediated by any number of factors. The proliferation of phenome-scale datasets allows researchers to simultaneously measure the effects of many possible mediators, enabling the conversion

---

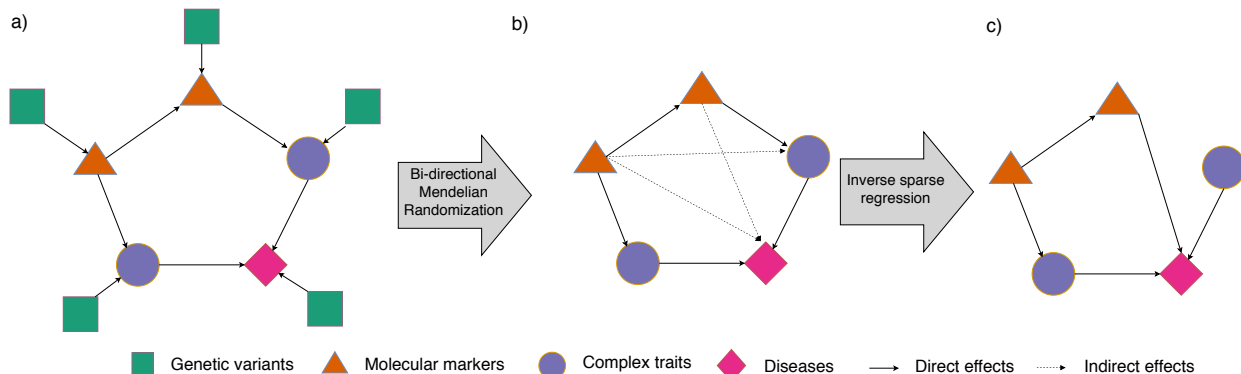[*]bb2991@columbia.edu
[†]dak2173@columbia.edu

Figure 1: a) Modern biobanks contains measurements of genetic variants (green squares), molecular markers (orange triangles), complex traits (purple circles) and diseases (pink diamonds). Genetic variants effect these phenotypes which in turn effect each other. b) Bi-directional Mendelian randomization estimates the total causal effect of the phenotypes on each other, which includes both direct (solid arrow) and indirect (dashed arrow) effects. c) The direct effects can be found by estimating a sparse approximate inverse to the matrix of total effects, a process we call inverse sparse regression.

of TCE estimates into causal direct effect (CDE) estimates, which are not mediated by any other measured factor. This raises another disadvantage of approaches such as LCV and gwas-pw . Assuming that either A causes B or B causes A, but not both, is equivalent to assuming that the underlying causal network lacks cycles, which are thought to be an important part of real biological networks (CITE ??).

> did you say what gwas-pw is?

Here, we introduce an approach called *bi-directional mediated Mendelian randomization* (bimmer) for inferring sparse networks of causal direct effects from phenome-scale GWAS summary statistics. Our approach has two parts. First, we perform bi-directional Mendelian randomization between every pair of phenotypes using Egger regression with a modified SNP selection and weighting scheme that dramatically reduces the influence of pleiotropic SNPs. This gives an estimate of the TCE of each phenotype on every other (Figure 1a-b). Second, we perform a causal mediation analysis to convert the matrix of total causal effects into a sparse, directed network of causal direct effects. We show that this can be modeled as an L_1-regularized matrix inverse problem, drawing analogy to the graphical lasso (CITE glasso), and introduce a new method for finding a sparse inverse to a partially-observed matrix called *inverse sparse regression* (inspre, Figure 1b-c). We show in extensive simulations that our approach is able to learn causal network structures even in the presence of non-causal genetic correlation. We apply our method to NNN phenotypes from the UK Biobank, finding thousands of direct and indirect causal effects.

2 Results

2.1 Overview of model

We model each phenotype as a function of 1) time-invariant genetic factors, 2) time-invariant environmental factors, and 3) other phenotypes at the previous time-point. Assume we have N individuals, D phenotypes and M SNPs, with Y_t be the matrix of phenotypes indexed by time t, X the genotype matrix, β the SNP effect matix and γ a matrix of unknown environmental effects. We denote by R the $D \times D$ matrix of causal direct effects, with $R_{i,j}$ the CDE of phenotype i on phenotype j. We assume that phenotypes do not effect themselves ($R_{i,i} = 0$), and that the network is sparse (R has many entries that are 0). Our goal is to estimate R given summary statistics for the association of the genotypes X with the phenotypes measured when the

2

system has reached equilibrium, $Y = Y_t$. Our trait model is

$$Y_{t+1} = Y_t R + X\beta + \gamma \tag{1}$$

which converges to $Y = (X\beta + \gamma)(I - R)^{-1}$ at equilibrium if the largest eigenvalue of R has magnitude below 1.

Let R^{TCE} be the matrix of TCE estimates from MR, with $R_{i,j}^{TCE}$ the total causal effect of phenotype i on phenotype j and $S_{i,j}$ it's standard error. We show 4 that in this model,

$$R = I - R^{TCE^{-1}} D[1/R^{TCE^{-1}}] \tag{2}$$

where D is an operator that sets all off-diagonal elements to 0, and / represents element-wise division.

In practice, the matrix R^{TCE} need not be well-conditioned or even invertible, leading to challenges when solving 2. Instead of calculating an exact or psuedo-inverse, we exploit the assumption that the underlying graph of CDE is sparse. Specifically, we seek matrices U and V such that $VU = I$, $U \approx R^{TCE}$ and V is sparse. We find them by solving the following constrained optimization problem,

$$\min_{\{U,V:VU=I\}} \frac{1}{2}||W \circ (R^{TCE} - U)||_F^2 + \lambda \sum_{i \neq j} |V_{ij}| \tag{3}$$

where $W = W_{i,j} = 1/S_{i,j}^2$ is a set of per-entry inverse variance weights, and λ is the LASSO shrinkage parameter (CITE LASSO, glasso). Note that in this method, missing entries in R^{TCE} can be accommodated simply by setting their weights to 0.

Some intuition for 2 can be gained by considering the problem of estimating a matrix of partial correlations for a set of observed variables. Analogous to the CDE, the partial correlation measures the degree to which two variables are correlated while controlling for the effect of all other measured variables. Given a matrix of observed (standard) correlations, Σ, the matrix of partial correlations is $P = D[\Sigma^{-1}]\Sigma^{-1}D[\Sigma^{-1}]$. One of the most common approaches to calculating Σ^{-1}, also called the precision matrix, is the graphical lasso (glasso). This method works by assuming the data come from a multivariate normal distribution with a sparse precision matrix, and maximizing the data likelihood with a LASSO penalty.

We choose the regularization parameter λ by randomly setting entries of the weight matrix to 0 and evaluating the stability of the resulting graph. This is analogous to the stability approach to regularization selection(CITE stars), except we exploit the ability of our method to handle missingness in R^{TCE} to induce variance in the graph rather than splitting the input matrices, which would require individual-level data. In each of 10 cross-validation iterations, we randomly set 20% of W to 0 and then use inspre to infer the matrix R for various values of λ. We use these results to estimate the probability that each edge is included in the graph under random masking, and use these probabilities to infer a stability score $\hat{D}$ - roughly corresponding to the fraction of times that two graphs with the same λ disagree on the inclusion of an edge, averaged over all edges. We set *lambda* to the largest value which gives a stability score $\hat{D} < 0.05$. For complete details see Section 4.

This leaves the problem of producing a good estimate for R^{TCE}, which can be challenging when there is non-causal genetic correlation or differential power across phenotypes. Most MR studies use the set of genome-wide significant (GWS, $p \leq 5 \times 10^{-8}$) SNPs for a trait as instruments. Instead, we exploit the observation that if A causes B and a SNP effects A directly, the effect of the SNP on B can be no larger than the effect of the SNP on A times the effect of A on B. That is, the SNP must have it's per-variance contribution to B reduced by the network. We use this intuition to construct a new weighting scheme for Egger regression. First, we select a p-value threshold p. For every phenotype i, we construct a set of marginally associated SNPs at threshold p. Next, for every ordered pair of phenotypes i, j, we consider only SNPs that reach signficance level p in phenotype i but not j. For this set of SNPs, we calculate a weight based on the Welch test statistic for a two-sample difference in mean and the standard inverse-variance weight. If $\hat{\beta}_{k,i}$ is our estimate of the effect of SNP k on phenotype i and $\hat{s}_{k,i}$ it's standard error, our weight is,

$$w_k^{i,j} = \frac{|\hat{\beta}_{k,i}| - |\hat{\beta}_{k,j}|}{\sqrt{\hat{s}_{k,j}^2(\hat{s}_{k,i}^2 + \hat{s}_{k,j}^2)}} \tag{4}$$

3

We use these SNP weights in the Egger regression of j on i. To avoid bias, this means that we must use two sets of summary statistics: one set for SNP selection and weight construction, and the second set for R^{TCE} estimation.

2.2 Simulations

Bi-directional Mendelian randomization

Our first goal was to assess whether our weighted Egger regression approach had a well-controlled type-I error rate (FPR) under the two-way null. To this end we simulated GWAS summary statistics for two phenotypes with $M = 1,000,000$ independent SNPs, 20% heritability and $N = 100,000$ individuals in both the SNP discovery and effect estimation cohorts. In each simulation, there were 5,000 causal SNPs per phenotype. In our first simulation, 1,000 of these SNPs are pleiotropic, effecting both phenotypes, but with no correlation of their effects. In our second, these 1,000 SNPs are again shared, but with correlated pleiotropy for a total genetic correlation of $\rho_g = 0.2$. In our final simulation under the null, we again have $\rho_g = 0.2$, except the studies have very different sample sizes ($N_1 = 200,000$, $N_2 = 50,000$) and shared effects are twice as large on average in the smaller cohort. This makes shared SNPs much more likely to have low p-values in the second cohort. In each setting, we compared our approach against the standard approach of Egger regression using all SNPs reaching GWS for the exposure as instruments, as well as an oracle with access to the true effect sizes that uses only non-pleiotropic SNPs.

In the first setting, uncorrelated pleiotropy, all methods were able to effectively control the FPR at level $\alpha = 0.05$ in both directions (Figure 2.2a, Table 4.4). In the second setting, correlated pleiotropy, standard Egger regression produced excess false-positives, but our weighting scheme is able to reduce the false positive rate substantially (Figure 2.2b, Table 4.4). In the most challenging setting, correlated pleiotropy with unequal power, standard Egger regression produces many excess false positives in both directions, but our weighting scheme again substantially reduces the error rate, from 0.284 to 0.087 in the $A \rightarrow B$ direction and from 0.492 to 0.029 in the $B \rightarrow A$ direction (Figure 2.2c, Table 4.4).

Next, we wanted to asses the power of our approach under the one-way alternate hypothesis for various effect sizes. We again conduct thee simulations, calculating the power for effect sizes ranging from 0.05 to 0.7. In the first, the cohorts had equal sample sizes. In the second, the exposure cohort has larger sample size, and in the third the outcome cohort has a larger sample size. In all settings, our weighted Egger approach shows a substantial gain in power over standard Egger regression. This is especially notable for smaller effect sizes, and when the outcome GWAS is larger. In this latter setting, the power of standard egger regression is only slightly higher than the FPR for the null hypothesis on the reverse direction, while our weighted Egger regression has very high power (Figure 2.2d-f, Table 4.4). However, both methods suffer from an increase in false positives in the reverse direction when the effect size in the forward direction is strong. For more on this phenomenon, see 3.

Finally, we tested the power of our approach under the two way alternate hypothesis. We tested pairs of effects ranging from -0.5 to 0.5 in both cohorts. Here we conduct two simulations: one with equal sample size of $N = 100,000$, and one unequal sample sizes $N_1 = 200,000$ and $N_2 = 50,000$. In all settings, our approach improves power substantially over standard Egger regression (Figure 2.2a-d). As with the one-way alt, this is particularly apparent when the outcome has a larger sample size than the exposure (Figure 2.2d). We also observed that both methods had lower power when $R_{12} \approx -R_{21}$ and vice versa, especially when both are large. Indeed, as $R_{12} \rightarrow -R_{21} \rightarrow 1$, the model becomes unidentifiable. This setting is actually a violation of the *faithfulness* assumption commonly employed in causal inference (CITE ??).

In these simulations, we used a p-value threshold of 5×10^{-6} for all wighted Egger regresssion analyses. We tested p-value thresholds ranging from 5×10^{-4} to 5×10^{-8}, and found similar results compared to standard Egger for all thresholds. We found that 5×10^{-6} provided a nice balance between increased power under the alt and control of the type-I error rate under the null. However, lower cutoffs will provide better control of the type-I error rate in difficult situations at the expense of reduced power. Like-wise, higher cut-offs yield higher power while reducing control of the type-I error rate (Tables 4.4 and 4.4).
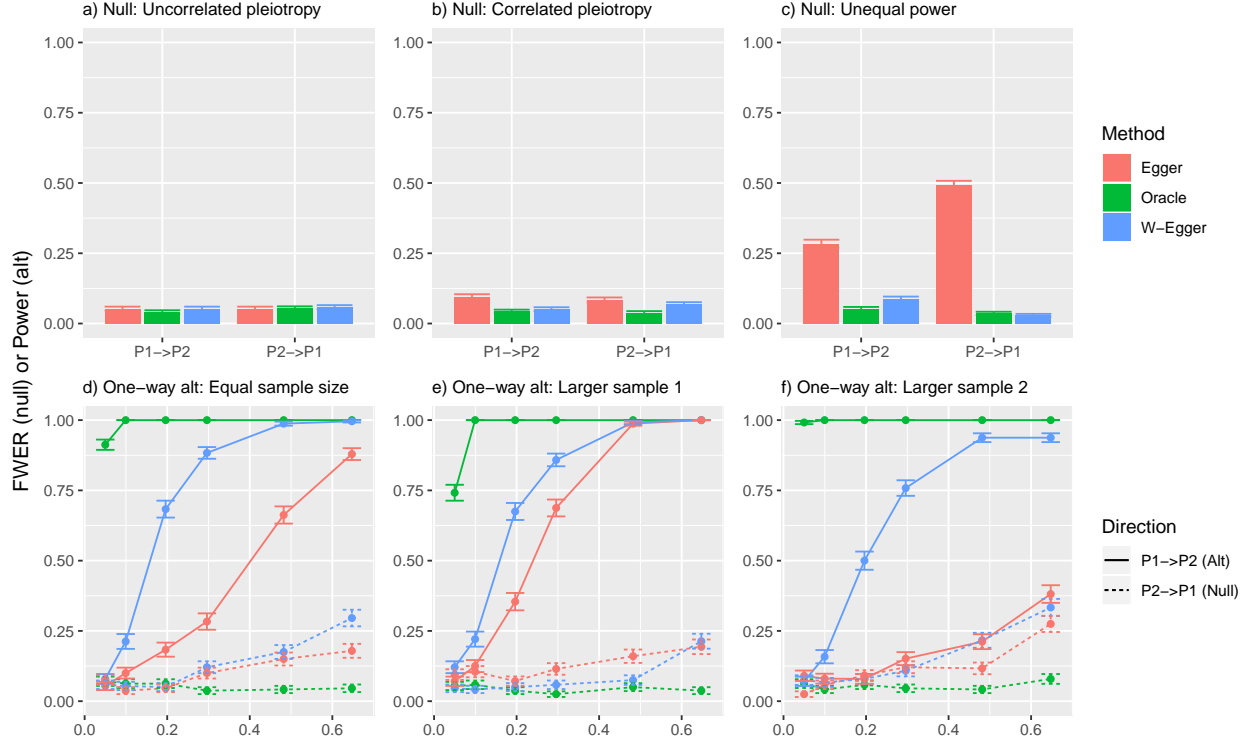
Figure 2: We simulated GWAS summary statistics for two phenotypes (A, B) with $M = 1,000,000$ independent SNPs, 20% heritability and $N = 100,000$ individuals in both the SNP discovery and effect estimation cohorts. In each simulation, there were $5,000$ causal SNPs per phenotype. a) Both the effect of A on B and B on A are null, and 1000 of the SNPs have uncorrelated pleiotropic effects. All methods are well behaved. b) Both effects are again null, but the 1000 shared SNPs have equal effects on both phenotypes. Egger regression results in excess false positives which our weighting scheme reduces. c) Both effects are null and the shared SNPs have an equal effect on both phenotypes, but the shared SNPs have twice as large an effect on B, which also has a much smaller sample size. Egger regression results in numerous false positives, which our weighting scheme corrects. d) A has a variable effect on B and the studies have equal sample size. Our weighting scheme improves power over standard Egger regression. e) A effects B, which has a much lower sample size. Our weighting scheme improves power, but not as much as in (d). f) A effects B, but A has a much smaller sample size. Our weighting scheme substantially increases power. We conduced 1000 simulations for each null experiment (a-c) and 250 simulations per effect size for each alt experiment (d-f).
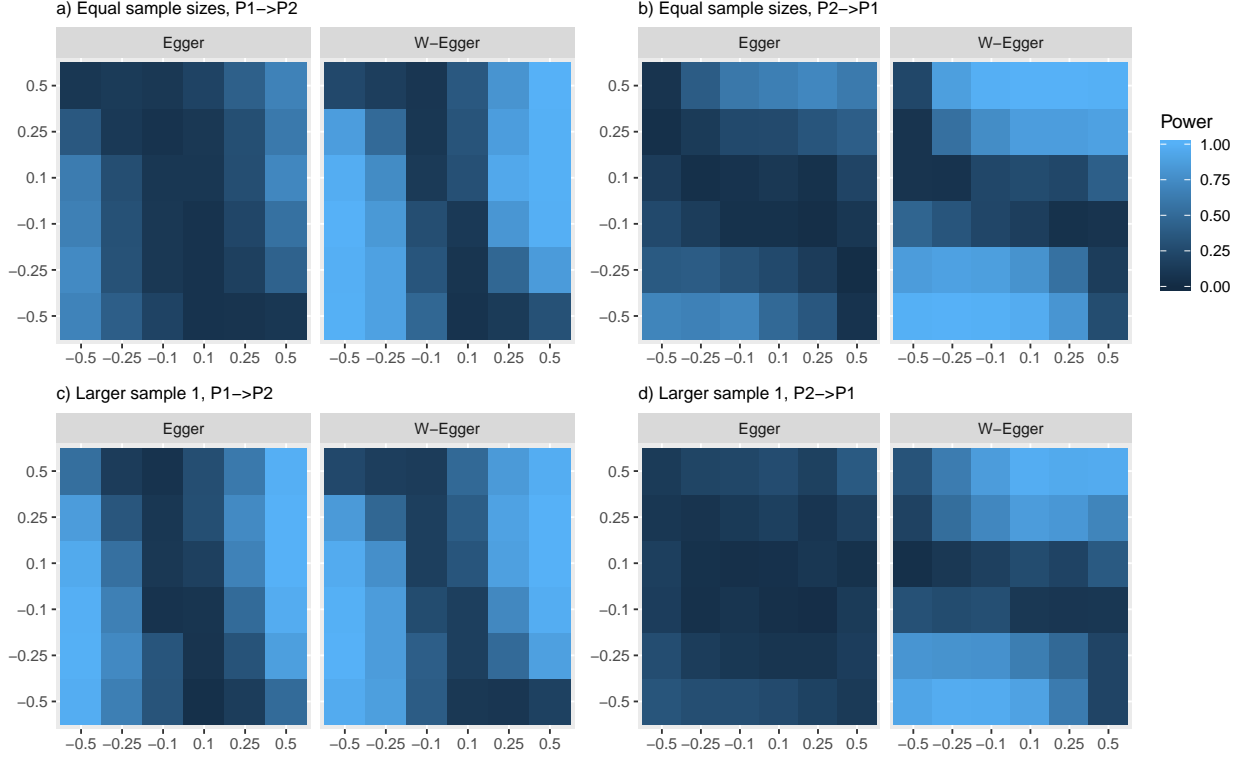
Figure 3: We simulated GWAS summary statistics for two phenotypes (A, B) with $M = 1,000,000$ independent SNPs, 20% heritability and $N = 100,000$ individuals in both the SNP discovery and effect estimation cohorts. In each simulation, there were $5,000$ causal SNPs per phenotype of which $1,000$ were shared with uncorrelated effect sizes. a) Power to detect the effect of A on B when the studies have equal sample sizes. Our weighting scheme increases power of standard Egger regression, but both methods struggle to detect when the traits cancel each other out. b) Power to detect the effect of B on A. Our approach improves power and the cancellation pattern is transposed. c) Power to detect the effect of A on B when A has a larger sample size. Our approach improves power, though both do well. d) Power to detect the effect of B on A when A has a larger sample size. Our approach improves power substantially over standard Egger regression, which struggles to detect the effect.

6

Inverse sparse regression

As detailed above, both inspre and glasso can be viewed as methods for finding a sparse, approximate inverse to a noisily measured matrix. Therefore, we sought to compare these two methods when data are simulated from the glasso model. We generated data from a multivariate-normal distribution with a sparse precision matrix for various graph structures, sample sizes, and numbers of features. We considered three kinds of graph structures: 1) Erdos-Reyni random graphs, where each edge is included with probability p, 2) hub graphs, where nodes are partitioned into disjoint sets and every node in each set is connected to a central "hub" vertex, 3) scale-free networks, where the vertex degree distribution follows a power law. Hub and scale-free networks are intended to mimic common biological networks (CITE ??). In each setting we calculated the precision, the number of true edges among all inferred edges, and recall, the proportion of true edges detected. We used these to calculate the F_1 score, the harmonic mean of precision and recall (CITE ??), as a function of the stability of the inferred graph. For the graphical lasso, we used StARS to evaluate graph stability. For inspre, we used random masks in the weight matrix as detailed above. As suggested in (CITE stars), we focus on the crucial region of stability around $\hat{D} = 0.05$.

First, we simulated data with 40 features and 800 samples. Our random graphs included each edge with probability $p = 0.04$, and our hub graphs had two hubs of 20 features each. In this setting inspre and glasso performed similarly for all graph types, with glasso performing slightly better on random graphs, inspre performing slightly better on hub graphs, and both methods having very similar performance for scale-free graphs (Supplmental Figure 4.4a-c). Next, we simulated data with 100 features and 500 samples. Here our random graphs included each edge with probability $p = 0.02$ and our hub graphs had 5 hubs. In this setting, glasso outperformed inspre on random graphs, inspre outperformed glasso on hub graphs, and both methods again had similar performance on scale-free graphs, with a slight edge towards glasso (Figure 4.4d-f).

We hypothesized that if the entries in the correlation matrix had variable sample sizes, the ability of inspre to incorporate weights would improve performance. This represents a common real-world setting in which some features are measured on many samples, and some are measured on only a few. In each simulation, we first chose a maximum missingness threshold m uniformly between 50% and 99%. Then we simulated data with 100 features and 2000 samples. For each feature, we uniformly chose a random number between 0 and m and set that proportion of the features samples to NA. We then calculated the sample correlation matrix using only samples where both features were measured per pair of features. In this setting, inspre was able to continue producing accurate results even with when the maximum misssingness was high. On the other hand, glasso was not able to produce results at all when there was high missingness, instead returning a matrix of NA values (Figure 4.4).

Bi-directional mediated Mendelian randomization

Our final goal was to show that bi-directional Mendelian randomization could be combined with inspre to fit networks of simulated phenotypes from phenome-scale GWAS summary statistics. At the time of this writing we are not aware of any other methods for this specific problem. However, there are a few approaches to related problems that could be applied. Specifically, the CDEs between multiple exposures and a single outcome can be calculated from a multiple regression of SNP effects on the outcome against SNP effects on the exposures (CITE mvmr). This approach can be used to find sparse effects by using a LASSO or elastic net regression (elnet-Egger). A more sophisticated approach, such as MR-Beyesian model averaging (MR-BMA), could also be applied (CITE MR-bma).

First, we simulated summary statistics for 50 phenotypes with 1000 shared and 2000 private causal effect SNPs per pair of phenotypes, $125,000$ total SNPs. Each phenotype had 20% heritability. The causal network underlying the phenotypes came from an Erdos-Reyni random graph with randomly oriented edges. We found that MR-BMA outperformed comparably to elnet-Egger, but that they both performed poorly compared to inspre. Moreover, MR-BMA took about 20 times longer than inspre to run with default parameter settings (Figure 4.4).

Next, we performed larger-scale simulations with 100 phenotypes and $250,000$ total SNPs. We again simulated data from Erdos-Reyni, hub, and scale-free networks. In this setting both the graph structure

and the orientation of the graphs edges are important variables to consider. The edge orientation will not necessarily be random: for example, master regulators would have very high out-degree but low in-degree (CITE ??). For all graph types, we tested three ways of orienting the edges in the graph: 1) randomly set the orientation of each edge (random), 2) preferentially orient edges towards high-degree nodes (towards), and 3) preferentially orient edges away from high-degree nodes (away). See Figure 2.2a-c for examples of different kinds of graphs with different edge orientations. We excluded MR-BMA from these simulations due to runtime concerns.

We found that bimmer was able to accurately re-construct all graph types and edge orientations considered, while elnet-Egger consistently had poor performance (Figure 2.2d-i, Figure 4.4). For random graphs, we found that edge orientation did not have an effect on the performance of bimmer. This is possibly because the node degree distribution doesn't have enough variance to have nodes that consistently pull edges towards or away from them in the latter scenarios. For scale-free and hub graphs, we found that bimmer performed better when high-degree nodes had edges oriented away from them (Figure 4.4). This is particularly interesting as it corresponds to the most likely real-world scenario (CITE ??).

2.3   Application to NNN traits from the UK Biobank

3   Discussion

As biobanks continue to grow in size and scope, new methods that are able to leverage their power while overcoming common pitfalls will be required. These datasets offer unprecedented opportunity to study the causal relationship between molecular markers, complex traits and diseases. We have introduced bi-directional mediated Mendelian randomization (bimmer), a novel approach to inferring sparse causal networks from phenome-scale GWAS summary statistics. We have shown through extensive simulations that bimmer is able to learn causal graph structures even in the presence of non-causal genetic correlation and differential power across phenotypes. We applied bimmer to NNN phenotypes from the UKBB and found...

While we are not aware of other methods for this problem, our approach builds on recent MR literature. In particular, multi-variable Mendelian randomization methods are able to compute causal direct effects when there are multiple potential exposures and a single outcome (CITE mvmr, MR-BMA). While these methods work well in that setting, we have shown that they are not well-suited to the more general problem that we consider here. Another approach, network Mendelian randomization, calculates the effect of an exposure on an outcome while accounting for the effects of a third variable (CITE netmr). Our method can be thought of as a generalization of this approach to an arbitrary number of phenotypes without pre-specifying any as exposures or outcomes. The first step in our method involves bi-directional MR with Egger regression weights that reduce the effect of pleiotropic SNPs. This is related to several recent methods. In particular, gwas-pc uses asymmetry in the effect size distributions to choose an effect direction between the two phenotypes. Similarly, LCV uses this asymmetry to fit a latent variable model, where imbalanced genetic correlation between the phenotypes and latent variable imply the effect direction. Compared to these methods, our approach offers several advantages. First, like LCV but unlike gwas-pc, our method controls the type-I error rate when there is non-causal genetic correlation and differential power. Second, like gwas-pc, but unlike LCV, our method estimates a quantity that is interpretable as the effect of one phenotype on the other. Finally unlike both, we are able to estimate both effect directions simultaneously, allowing our model to accomodate graphs with cycles.

However, our approach also has several disadvantages. First, our method requires that we split the initial cohort into instrument discovery and effect estimation sub-cohorts. This is common in MR methods, but LCV has the distinct advantage of using all SNPs, which obviates the need for sample splitting and might improve power. Second, while there are some phenotype pairs where a direct cause makes sense, there are others where causality is almost certainly better modeled as the action of a latent variable. Indeed, it is likely that some of the causal effects we infer actually represent shared causal pathways. Finally, our method suffers from an increase in false positives in the $B \to A$ direction when there is a strong effect from $A \to B$. When there are many causal SNPs and the effect of A on B is strong, some SNPs that directly effect A can be
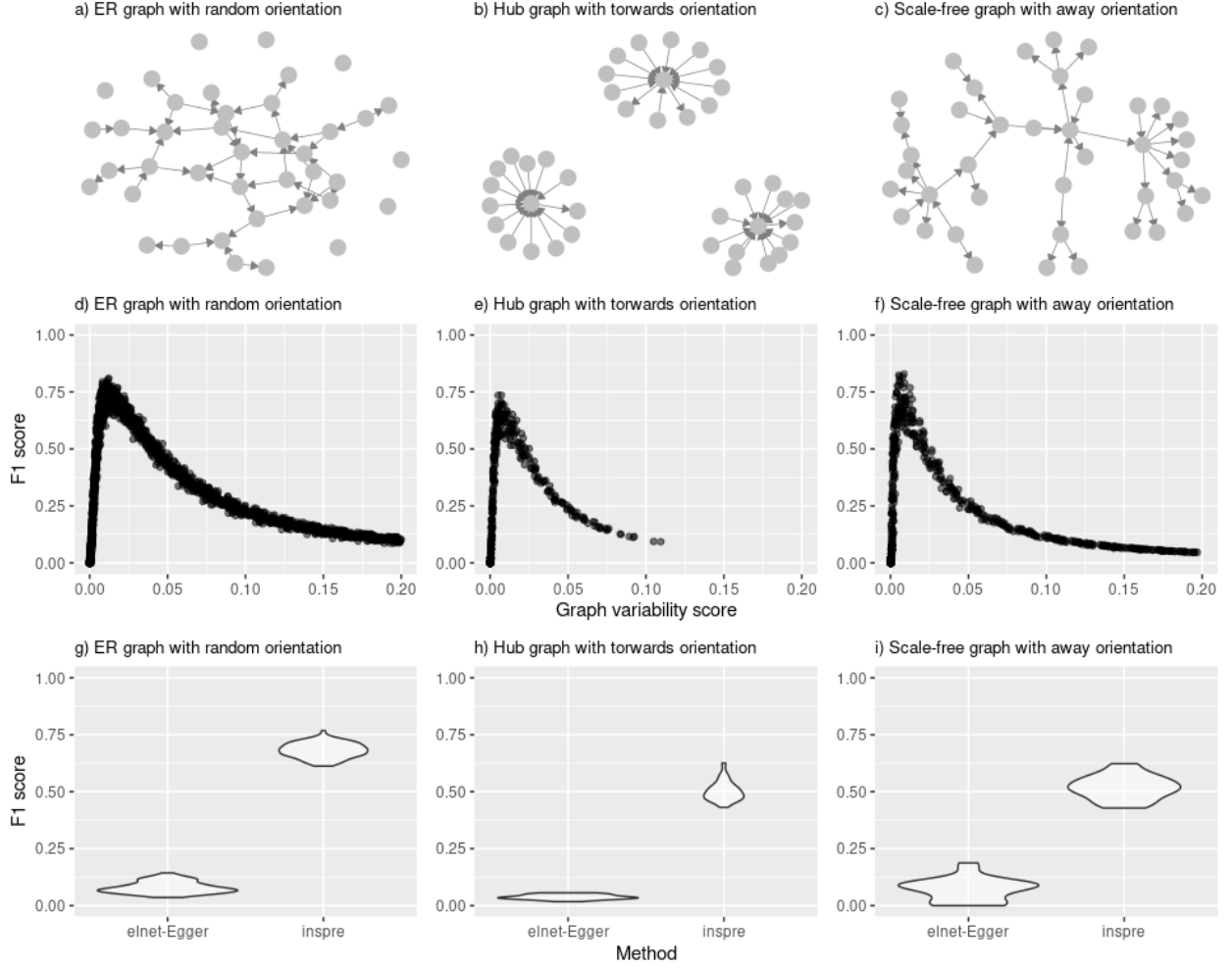
Figure 4: We simulated summary statistics for 100 phenotypes with 3000 causal effects each, 1000 of which were shared with uncorrelated effects per pair of phenotypes. We varied the structure and edge orientation of the causal graph underlying the phenotypes. a) An Erdos-Reyni random graph with randomly oriented edges. Each edge is included with probability $p = 0.05$ and then randomly assigned an orientation. b) A hub graph with edges preferentially oriented towards high degree nodes. The nodes are split into three sets and each node in each set is assigned to a central hub vertex. c) A scale-free graph with edges preferentially oriented away from high degree nodes. These graphs have node degrees that follow a power-law distribution. We show the F_1-score of the method against the calculated variability score for d) random, e) hub and f) scale-free graphs. In all cases, we are able to produce accurate results when the variability score is between about 0.01 and 0.05. We also compared the performance against Egger regression with elastic-net shrinkage at a graph variability score of 0.025. elnet-Egger performs quite poorly compared to bimmer.

mistakenly used as instruments for the effect of B on A. While our method reduces the magnitude of this estimated effect, it can still give some false positives. Our approach also still suffers from the small-effect bias, generally underestimating the causal effect, which reduces power (CITE raps?). We view the development of MR methods that utilize the entire spectrum of GWAS results and are capable of being used for network inference as an important area for future work.

The second step of our method involves finding a sparse inverse to a noisily measured matrix, and is therefore closely related to the graphical lasso. Like glasso, our method also has a single regularization parameter than can be set in a straightforward manner. However, a key advantage of our approach is that we are able to incorporate weights. This is extremely important in our application since the standard errors of the TCE matrix can vary dramatically. This also allows us to approximately invert matrices with missing data, implicitly performing matrix completion by leveraging assumed structure in the inverse of the matrix. Another advantage of this approach is that it allows us to select the lasso parameter λ without access to the underlying data. A final advantage is that this step in our approach makes no assumptions about the data generating process. We found that for many classes of graphs, inspre and glasso produced similar results, however there were some settings where glasso clearly performed better. Moreover, our method is substantially slower than glasso, with complexity $O(??)$ compared to glassos $O(??)$. In spite of these limitations, we believe the advantages of our method for graph inference mean that it will find utility well-outside the scope of MR, and we view this as an important avenue for future work.

Another advantage of our approach is that it only requires GWAS summary statistics. While the UK BioBank primary genotypes and phenotypes are readily available, summary statistics are much easier to share and faster to work with when the primary data is large. They also enable researchers to work with data from a standardized analysis pipeline (CITE neale lab website). Strictly speaking, our method does not even require summary statistics. If MR analysis results are already available for every pair of a set of phenotypes, the matrix R^{TCE}

In this work we have begun to elucidate the connection between Mendelian randomization and omnigenics. The effects of genetic variants can be used to find and orient edges in the causal graph underlying the phenotypes, and long-range effects can be modeled as paths in this sparse graph. Our method can be applied well beyond the scope considered here. We are particularly interested in the application to datasets of molecular phenotypes. These datasets generally have much smaller sample sizes, but molecular phenotypes also tend to be less polygenic with larger SNP effect sizes, which improves the efficiency of MR. Inverse sparse regression could also be applied to datasets from CRISPR-based genetic perturbation experiments, where it might improve the accuracy of network estimation. We view all of these applications as important avenues for future work.

4 Methods

4.1 Trait model

As detailed above, our goal is to estimate a sparse causal graph, R, from summary association statistics between genotypes X and phenotypes Y. We model the SNP effects β and the causal graph as fixed, and assume that the genotypes X are sampled uniformly from a population. For convenience, we assume throughout that SNPs and phenotypes have been normalized to have mean 0 and variance 1. We also assume that SNPs are uncorrelated (no LD) and use LD-pruned variants in all analyses of real data. Consider fitting the above model $Y = (X\beta + \gamma)(I - R)^{-1} + \epsilon$ using two-stage least-squares with X as instruments. For now, assume each SNP acts only on one phenotype (there is no pleiotropy) and that we know which phenotype it is. First regress each instrument on it's phenotype and use these effect estimates to calculate a set of phenotype scores for each individual. Next, regress each phenotype score on the observed values of the other phenotypes, creating a matrix containing estimates of the total causal effect (TCE) of each phenotype on

every other. This gives observed effect matrix $\hat{\beta}$,

$$\hat{\beta}_{ij} = \begin{cases} \frac{1}{N}X_{:,i}^\top Y_{:,j} & |\beta_{i,j}| > 0 \\ 0 & otherwise \end{cases}$$

$$\mathbb{E}[\hat{\beta}] = \beta(I - R)^{-1} \circ \mathbb{1}[|\beta| > 0]$$

where $\mathbb{1}$ is an indicator function and $\circ$ is the Hadamard matrix product. The TCE matrix is then given by

$$\hat{R}^{TCE} = \frac{1}{N}(X\hat{\beta})^\top Y$$

$$= \frac{1}{N}(X\hat{\beta})^\top YR + \frac{1}{N}(X\hat{\beta})^\top X\beta + \frac{1}{N}(X\hat{\beta})^\top \gamma + \frac{1}{N}(X\hat{\beta})^\top \epsilon$$

$$\mathbb{E}[\hat{R}^{TCE}] = \mathbb{E}[R^{TCE}]R + D[\beta(I - R)^{-1}]$$

where the diagonal operator $D[X]_{i,j} = \begin{cases} X_{i,j} & i = j \\ 0 & i \neq j \end{cases}$ sets off-diagonal elements of a matrix to 0. Since $\mathbb{E}[\hat{R}^{TCE}] = R^{TCE}$, this tells us that R^{TCE} satisfies the recurrence $R^{TCE} = R^{TCE}R$ off the diagonal, from which it follows that [4],

$$R = I - R^{TCE^{-1}}D[1/R^{TCE^{-1}}] \tag{5}$$

where / indicates elementwise division.

In practice we don't know which SNP effects which phenotype, and there can be correlated pleiotropic effects. Intuitively, non-pleiotropic SNPs will obey the relationship

$$\beta_{k,j} \approx \beta_{k,i}R_{i,j} \tag{6}$$

thereby contributing $\beta_{k,i}^2 R_{i,j}^2$ to the variance of Y_j, whereas pleiotropic SNPs will contribute $\beta_{k,i}^2 R_{i,j}^2 + \alpha^2$ for some pleiotropic effect size α. Therefore, SNPs that appear to have a larger absolute effect on the exposure relative to the out in a discovery cohort are more likely to satisfy 6. First, we split the samples into discovery and estimation sets, generating two sets of summary statistics $\hat{\beta}_{dis}, \hat{s}_{dis}$ and $\hat{\beta}_{est}, \hat{s}_{est}$. Next, for each phenotype i we identify the set of SNPs marginally associated at p-value threshold p. Call this set $I_i = \{k : \hat{p}_{k,i} < p\}$. For every SNP $k \in I_i$ and every phenotype j, we calculate the weight for SNP k in the regression of j on i as $w_k^{i,j} = \frac{|\hat{\beta}_{k,i}| - |\hat{\beta}_{k,j}|}{\sqrt{\hat{s}_{k,j}^2(\hat{s}_{k,i}^2 + \hat{s}_{k,j}^2)}}$. This is best on the Welch test for a two-sample difference in mean (CITE ??).

4.2 Inverse sparse regression

If we knew R^{TCE} exactly, we could simply invert it and plug the inverse into 5. However, our estimate $\hat{R}^{TCE}$ is not necessarily well-conditioned or even invertable. Instead observe that in 5, R is sparse if and only if $\hat{R}^{TCE^{-1}}$ is sparse, and so we can think of solving 5 as finding a sparse matrix inverse. Let A be an arbitrary $D \times D$ matrix. We seek matrices U, V with $VU = I$ that minimize the loss,

$$\frac{1}{2}||W \circ A - U||_F^2 + \lambda \sum_{i \neq j} |V_{ij}| \tag{7}$$

We minimize this loss using alternating direction method of multipliers (ADMM) [1]. Let Θ^k be a matrix of Lagrange multipliers. The updates for U^k, V^k and Θ^k are

$$V^{k+1} \leftarrow \arg\min_V \left\| \frac{1}{\sqrt{\rho}}\left(I - \theta^{k^\top}\right) - \sqrt{\rho}U^{k^\top}V^k \right\|_F^2 + \lambda \sum_{i \neq j} |V_{ij}^k| \tag{8}$$

$$U_{:,d}^{k+1} \leftarrow \left(\rho V^{k+1^\top}V^{k+1} + D[W_{:,d}]\right)^{-1}\left(\rho V_{:,d}^{k+1^\top} - \left(V^{k+1^\top}\theta\right)_{:,d} + (W \circ A)_{:,d}\right) \tag{9}$$

$$\theta^{k+1} \leftarrow \theta_k + \rho(V_{k+1}U_{k+1} - I) \tag{10}$$

11

where ρ is the penalty parameter (CITE admm). The first of these can be solved with a straightforward LASSO regression. For the second, we use the bigconjugate gradient stabilized method implemented in the Rlinsolve package to solve the linear system rather than explicitly computing the inverse (CITE Rlinsolve). We always start from the initial condition $U_0 = V_0 = I$. For the derivation of these equations including the specifics of how we set the penalty parameter see 4.4.

4.3 Setting the LASSO penalty

Let ϕ_λ be a $D \times D$ matrix where entry i, j is the probability that each edge i, j is included in the graph for regularization setting λ. Our goal is to estimate ϕ_λ for many choices of λ and turn this into a graph instability measure D_λ. Let $W_{i,j}^k = W_{i,j}$ with probability p and $W_{i,j}^k = 0$ with probability $1 - p$. Let $V_\lambda^k = f(A, W^k, \lambda)$ be the function approximating the inverse of A for regularization setting λ and weight set W^k. Let $\psi_\lambda^k = \mathbb{1}[V_\lambda^k > 0]$. Then ϕ_λ can be estimated as

$$\hat{\phi}_\lambda = \frac{1}{K} \sum_{k=1}^{K} \psi_\lambda^k \tag{11}$$

using K independent random masks. Now let $\hat{\xi}_{i,j}^\lambda =$. The instability measure D_λ is estimated as [3]

$$\hat{D}_\lambda = \frac{1}{D(D-1)} \sum_{i,j} 2\hat{\phi}_\lambda^{i,j}(1 - \hat{\phi}_\lambda^{i,j}) \tag{12}$$

Clearly, $D = 0$ for very large values of λ, where $V_\lambda^k = I$ for every mask k. As λ becomes smaller, D rises, but as lambda approaches 0, $D \to 0$ as $V_\lambda^k \to A^+$. Following [3], we first normalize $\hat{D}_\lambda$ by setting it to $\bar{D}_\lambda = \sup_{l \le \lambda} \hat{D}_l$ and then choose the smallest value of lambda with stability below a cut point b, $\hat{\lambda} = \sup\{\lambda : \bar{D}_\lambda \le b\}$.

4.4 UK Biobank analysis

References

[1] Stephen Boyd, Neal Parikh, Eric Chu, Borja Peleato, and Jonathan Eckstein. Distributed optimization and statistical learning via the alternating direction method of multipliers. *Foundations and Trends in Machine Learning*, 3(1):1–122, 2010.

[2] Jerome Friedman, Trevor Hastie, and Robert Tibshirani. Sparse inverse covariance estimation with the graphical lasso. pages 1–14, 2007.

[3] Han Liu, Kathryn Roeder, and Larry Wasserman. Stability approach to regularization selection (StARS) for high dimensional graphical models. *Advances in Neural Information Processing Systems 23: 24th Annual Conference on Neural Information Processing Systems 2010, NIPS 2010*, pages 1–14, 2010.

[4] Lior S Pachter. The network nonsense of Albert-László Barabási — Bits of DNA.

Supplemental Note

Alternating direction method of multipliers

First, consider the unweighted optimization problem

$$\frac{1}{2}||A - U||_F^2 + \lambda \sum_{i \ne j} |V_{ij}| \tag{13}$$

The augmented Lagrangian is,

$$L = \frac{1}{2}||A - U||_F^2 + \lambda \sum_{i \neq j} |V_{ij}| + \mathrm{Tr}(\theta(VU - I)) + \frac{1}{2}\rho||VU - I||_F^2$$

The update for V can be found by noticing that minimizing L is equivalent to solving a lasso regression with design matrix $\sqrt{\rho}U^\top$ and response $\frac{1}{\sqrt{\rho}}(I - \theta^\top)$,

$$L \propto \mathrm{Tr}(\theta(VU - I)) + \frac{1}{2}\rho||VU - I||_F^2 + \lambda \sum_{i \neq j} |V_{ij}|$$

$$= ||\frac{1}{\sqrt{\rho}}(I - \theta^\top) - \sqrt{\rho}U^\top V||_F^2 + \lambda \sum_{i \neq j} |V_{ij}|$$

The update for U can be found by taking the gradient $\nabla_U L$ and setting it to 0,

$$\nabla_U L = A - U + V^\top \theta + \rho V^\top(VU - I)$$
$$U = (I + \rho V^\top V)^{-1}(A + \rho V^\top - V^\top \theta)$$

ADMM gives the update for θ [1],

$$\theta \leftarrow \theta + \rho(VU - I) \tag{14}$$

Now we consider the weighted version. Assume that in addition to the matrix A, we also have a matrix of standard errors of the entries of A, S_A. Let $W = 1/S_A^2$ be a matrix of inverse variance weights. We now seek matrices U, V with $VU = I$ that minimize the loss,

$$\frac{1}{2}||W \circ (A - U)||_F^2 + \lambda \sum_{i \neq j} |V_{ij}| \tag{15}$$

This does not effect the update for V, however the gradient of the augmented Lagrangian with respect to U is now,

$$\nabla_U L = -W \circ (A - U) + V^\top \theta + \rho V^\top VU - \rho V^\top$$

which separates over columns of U, giving the update

$$U_{:,d} = (\rho V^\top V + D[W_{:,d}])^{-1}(\rho V_{:,d}^\top - (V^\top \theta)_{:,d} + (W \circ A)_{:,d}) \tag{16}$$

where here the D operator creates a matrix with $W_{:,d}$ on the diagonal and 0 elsewhere.

ADMM also requires that we set the parameter ρ, which controls the balance in the objective between the primal and dual constraints [1]. We follow standard practice of setting rho to an initial value and increasing or decreasing it according to the ratio of the solution to the primal and dual feasibility constraints. The primal residual at iteration $k+1$ is given by $r^{k+1} = V^{k+1}U^{k+1} - I$. The dual residual is found by setting $\nabla_U L^k = 0$ and evaluating it at U_{k+1}

$$\nabla_U L^k = A - U^{k+1} + V^{k^\top}\theta^k + \rho V^{k^\top}(V^k U^{k+1} - I)$$

$$= A - U^{k+1} + V^{k^\top}\theta^k + \rho V^{k^\top}r^{k+1} + \rho V^{k^\top}(V^k U^{k+1} - V^{k+1}U^{k+1})$$

$$= A - U^{k+1} + V^{k+1^\top}\theta^{k+1} + \rho V^{k^\top}(V^k - V^{k+1})U^{k+1}$$

Therefore the dual residual is [1]

$$d_k = \rho V^{k^\top}(V^k - V^{k+1})U^{k+1}$$

and we can adjust ρ as follows,

$$\rho^{k+1} = \begin{cases} \tau \rho^k & if \quad ||r^k||_2 > \mu||d^k||_2 \\ \rho^k/\tau & if \quad ||d^k||_2 > \mu||r^k||_2 \\ \rho^k & otherwise \end{cases}$$

which reduces the impact of the initial choice of ρ. While this may appear to be a lot of parameters, they effect the convergence of the algorithm substantially more than the solution obtained. We always use the default values $\rho = 10$, $\mu = 10$, $\tau = 2$.
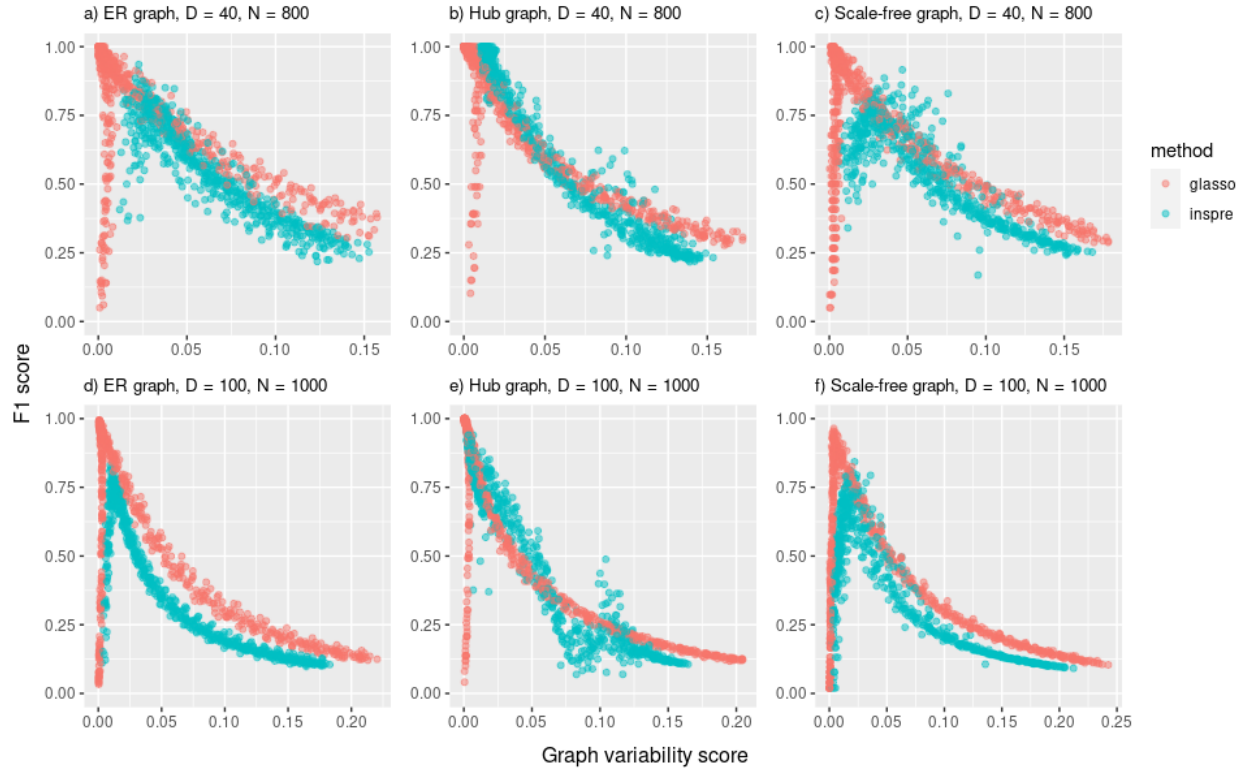
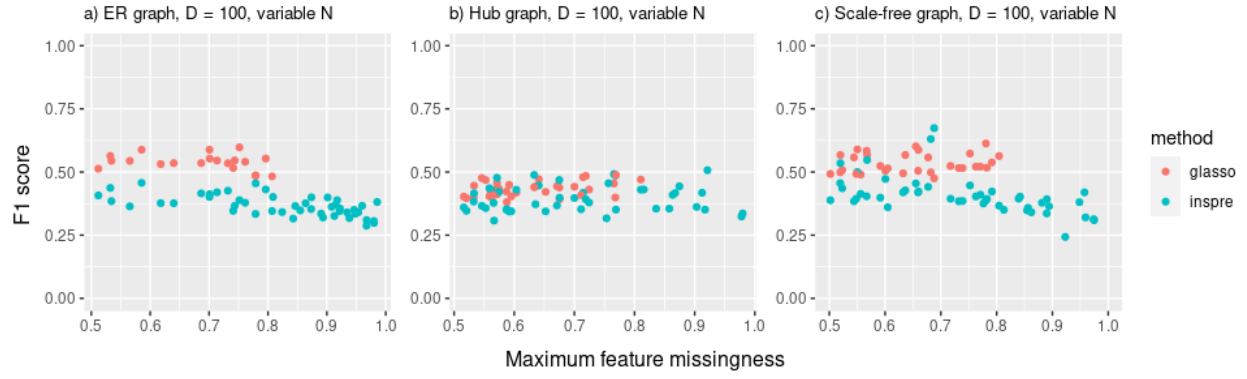Figure S1: Simulations comparing inspre and glasso for various graph stuctures.

Figure S2: Simulations comparing inspre and glasso for various graph stuctures with variable per-phenotype sample size.
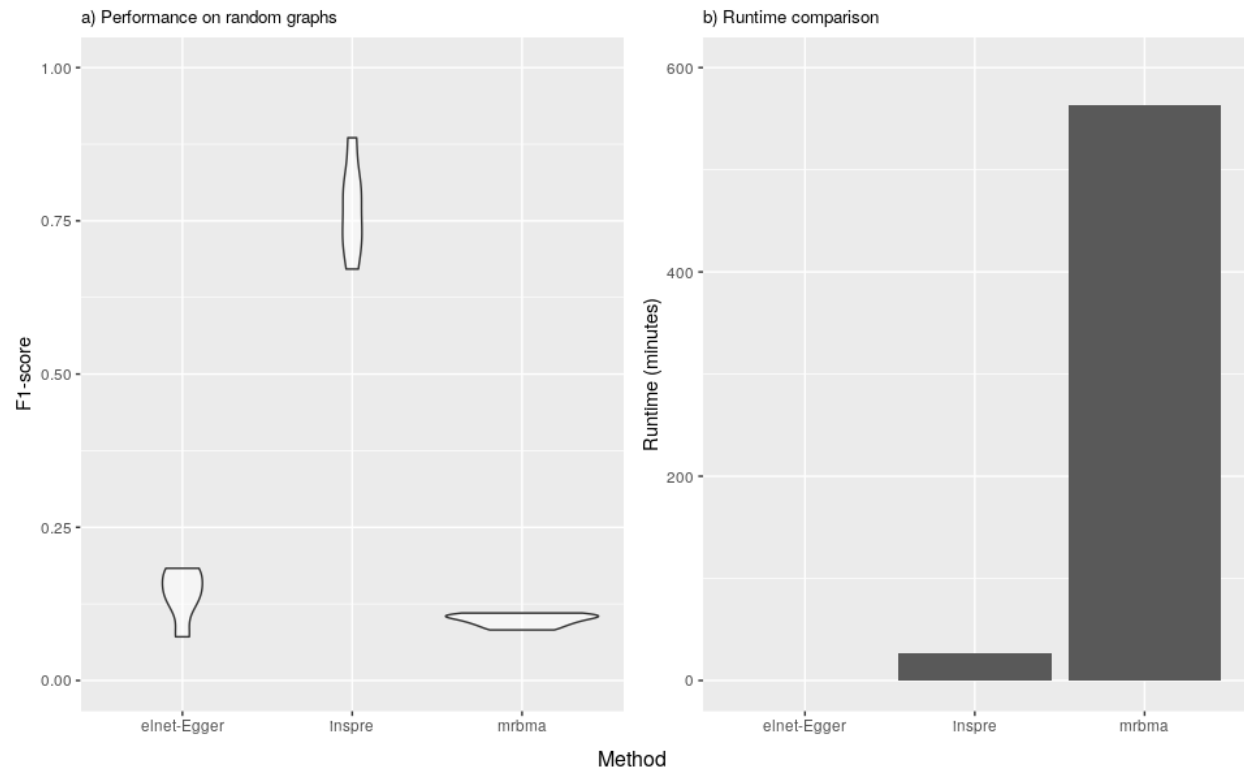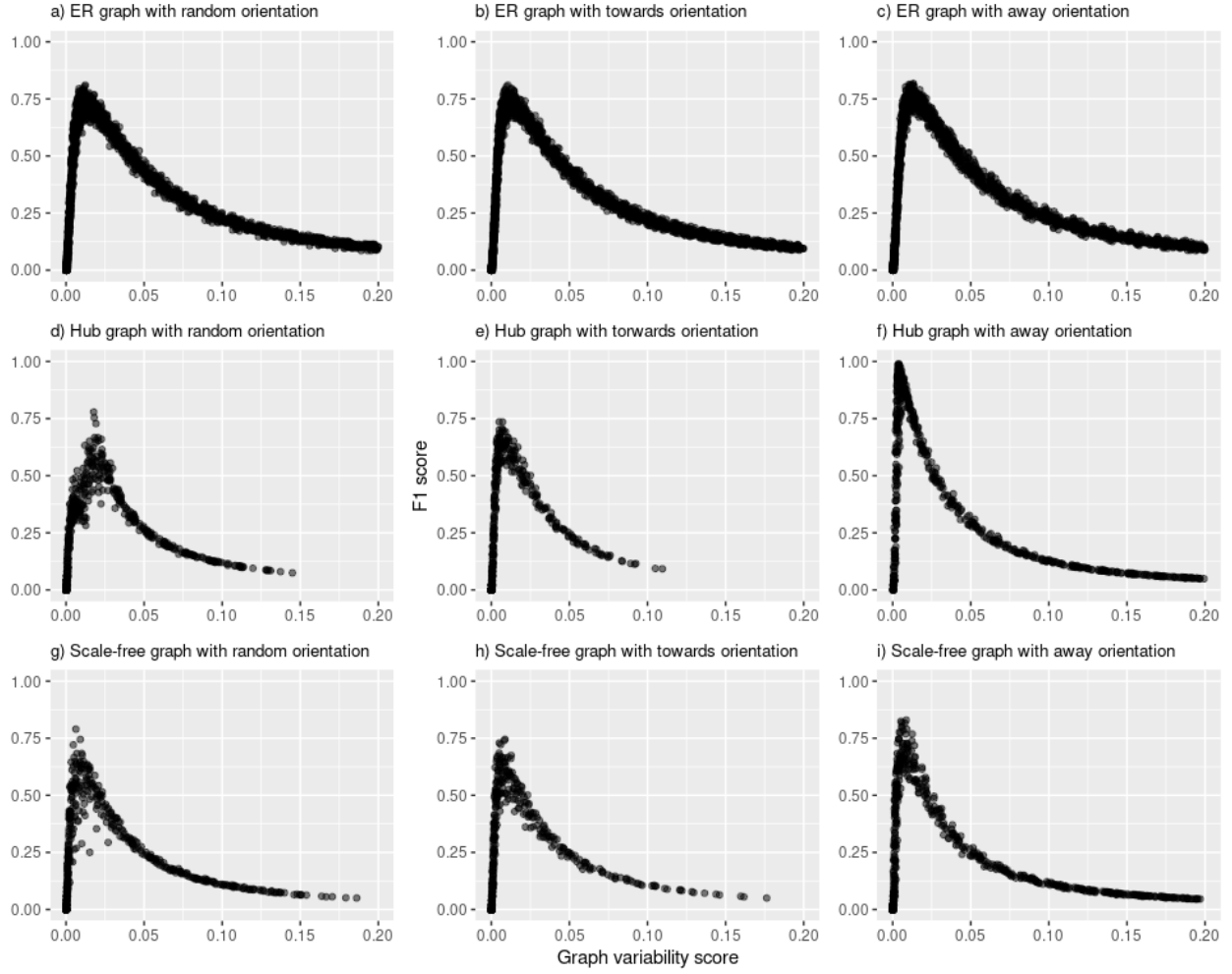
Figure S3: Simulations.

Figure S4: Simulations comparing inspre and glasso for various graph stuctures with variable per-phenotype sample size.

Method	stat1	se_stat1	stat2	se_stat2	mae1	se_mae1	mae2	se_mae2
Null: Uncorrelated pleiotropy								
Oracle	0.041	0.006	0.054	0.007	0.009	0.000	0.009	0.000
W-Egger	0.053	0.007	0.058	0.007	0.042	0.001	0.042	0.001
Egger	0.053	0.007	0.053	0.007	0.091	0.002	0.090	0.002
Null: Correlated pleiotropy								
Oracle	0.043	0.006	0.038	0.006	0.009	0.000	0.009	0.000
W-Egger	0.051	0.007	0.068	0.008	0.044	0.001	0.047	0.001
Egger	0.095	0.009	0.084	0.009	0.172	0.004	0.166	0.004
Null: Correlated pleiotropy, unequal power								
Oracle	0.052	0.007	0.036	0.006	0.014	0.000	0.006	0.000
W-Egger	0.087	0.009	0.029	0.005	0.053	0.001	0.080	0.002
Egger	0.284	0.014	0.492	0.016	0.178	0.003	0.648	0.010

Table S1: Simulations under the two-way null.

p_thresh	stat1	se_stat1	stat2	se_stat2	mae1	se_mae1	mae2	se_mae2
Null: Uncorrelated pleiotropy								
5e-04	0.070	0.008	0.073	0.008	0.016	0.000	0.016	0.000
5e-05	0.051	0.007	0.060	0.008	0.026	0.001	0.028	0.001
5e-06	0.053	0.007	0.058	0.007	0.042	0.001	0.042	0.001
5e-07	0.055	0.007	0.072	0.008	0.059	0.001	0.061	0.001
5e-08	0.059	0.007	0.059	0.007	0.081	0.002	0.077	0.002
Null: Correlated pleiotropy								
5e-04	0.075	0.008	0.074	0.008	0.017	0.000	0.017	0.000
5e-05	0.042	0.006	0.051	0.007	0.027	0.001	0.027	0.001
5e-06	0.051	0.007	0.068	0.008	0.044	0.001	0.047	0.001
5e-07	0.041	0.006	0.064	0.008	0.065	0.002	0.066	0.002
5e-08	0.039	0.006	0.058	0.007	0.088	0.002	0.088	0.002
Null: Correlated pleiotropy, unequal power								
5e-04	0.078	0.008	0.366	0.015	0.039	0.001	0.033	0.001
5e-05	0.086	0.009	0.144	0.011	0.045	0.001	0.050	0.001
5e-06	0.087	0.009	0.029	0.005	0.053	0.001	0.080	0.002
5e-07	0.073	0.008	0.049	0.007	0.060	0.001	0.187	0.006
5e-08	0.067	0.008	0.075	0.008	0.067	0.002	0.373	0.013

Table S3: Simulations under the two-way null for various p-value thresholds.

Method	stat1	se_stat1	stat2	se_stat2	mae1	se_mae1	mae2	se_mae2
Alt: Equal sample sizes, R=0.2								
Oracle	1.000	0.000	0.062	0.016	0.040	0.001	0.010	0.000
W-Egger	0.683	0.030	0.050	0.014	0.075	0.003	0.046	0.002
Egger	0.183	0.025	0.046	0.014	0.114	0.005	0.099	0.005
Alt: Equal sample sizes, R=0.5								
Oracle	1.000	0.000	0.042	0.013	0.095	0.001	0.010	0.000
W-Egger	0.988	0.007	0.175	0.025	0.189	0.004	0.086	0.004
Egger	0.662	0.031	0.150	0.023	0.229	0.007	0.215	0.010
Alt: Larger sample 1, R=0.2								
Oracle	1.000	0.000	0.038	0.012	0.024	0.001	0.006	0.000
W-Egger	0.675	0.030	0.050	0.014	0.070	0.003	0.054	0.003
Egger	0.354	0.031	0.071	0.017	0.083	0.004	0.190	0.013
Alt: Larger sample 1, R=0.5								
Oracle	1.000	0.000	0.050	0.014	0.055	0.001	0.007	0.000
W-Egger	0.992	0.006	0.075	0.017	0.148	0.005	0.086	0.004
Egger	0.988	0.007	0.160	0.024	0.166	0.005	0.520	0.032
Alt: Larger sample 2, R=0.2								
Oracle	1.000	0.000	0.058	0.015	0.065	0.001	0.015	0.001
W-Egger	0.500	0.032	0.079	0.017	0.077	0.004	0.052	0.003
Egger	0.079	0.017	0.092	0.019	0.237	0.017	0.068	0.004
Alt: Larger sample 2, R=0.5								
Oracle	1.000	0.000	0.042	0.013	0.161	0.001	0.015	0.001
W-Egger	0.938	0.016	0.217	0.027	0.161	0.006	0.097	0.004
Egger	0.212	0.026	0.117	0.021	0.319	0.015	0.116	0.006

Table S2: Simulations under the one-way alt.

p_thresh	stat1	se_stat1	stat2	se_stat2	mae1	se_mae1	mae2	se_mae2
Alt: Equal sample sizes, R=0.2								
5e-04	1.000	0.000	0.150	0.023	0.023	0.001	0.020	0.001
5e-05	0.988	0.007	0.079	0.017	0.048	0.002	0.031	0.001
5e-06	0.683	0.030	0.050	0.014	0.075	0.003	0.046	0.002
5e-07	0.375	0.031	0.042	0.013	0.089	0.004	0.064	0.003
5e-08	0.246	0.028	0.033	0.012	0.102	0.005	0.083	0.004
Alt: Equal sample sizes, R=0.5								
5e-04	1.000	0.000	0.596	0.032	0.058	0.002	0.051	0.002
5e-05	1.000	0.000	0.288	0.029	0.108	0.003	0.065	0.002
5e-06	0.988	0.007	0.175	0.025	0.189	0.004	0.086	0.004
5e-07	0.850	0.023	0.142	0.023	0.229	0.006	0.120	0.006
5e-08	0.612	0.032	0.079	0.017	0.239	0.008	0.155	0.007
Alt: Larger sample 1, R=0.2								
5e-04	0.929	0.017	0.133	0.022	0.050	0.002	0.018	0.001
5e-05	0.812	0.025	0.058	0.015	0.060	0.003	0.028	0.001
5e-06	0.675	0.030	0.050	0.014	0.070	0.003	0.054	0.003
5e-07	0.467	0.032	0.046	0.014	0.078	0.004	0.107	0.006
5e-08	0.358	0.031	0.062	0.016	0.087	0.004	0.161	0.010
Alt: Larger sample 1, R=0.5								
5e-04	1.000	0.000	0.433	0.032	0.095	0.003	0.037	0.001
5e-05	1.000	0.000	0.242	0.028	0.118	0.004	0.055	0.002
5e-06	0.992	0.006	0.075	0.017	0.148	0.005	0.086	0.004
5e-07	0.958	0.013	0.085	0.018	0.157	0.005	0.185	0.010
5e-08	0.896	0.020	0.104	0.020	0.165	0.006	0.334	0.018
Alt: Larger sample 2, R=0.2								
5e-04	1.000	0.000	0.092	0.019	0.039	0.001	0.041	0.002
5e-05	1.000	0.000	0.088	0.018	0.043	0.002	0.045	0.002
5e-06	0.500	0.032	0.079	0.017	0.077	0.004	0.052	0.003
5e-07	0.162	0.024	0.096	0.019	0.135	0.006	0.058	0.003
5e-08	0.080	0.018	0.088	0.018	0.216	0.012	0.066	0.003
Alt: Larger sample 2, R=0.5								
5e-04	1.000	0.000	0.246	0.028	0.146	0.002	0.072	0.003
5e-05	1.000	0.000	0.212	0.026	0.098	0.003	0.078	0.003
5e-06	0.938	0.016	0.217	0.027	0.161	0.006	0.097	0.004
5e-07	0.435	0.032	0.183	0.025	0.259	0.011	0.106	0.005
5e-08	0.150	0.023	0.146	0.023	0.343	0.016	0.118	0.006

Table S4: Simulations under the one-way alt for various p-value thresholds.